Journal of Applied Fluid Mechanics, Vol. 9, No. 6, pp. 2731-2741, 2016.
Available online at www.jafmonline.net, ISSN 1735-3572, EISSN 1735-3645.
DOI: 10.29252/jafm.09.06.25330

Large Eddy Simulation of the Flow-Field around Road Vehicle Subjected to Pitching Motion

Z. Q. Gu[1,3], T. M. Huang[1,2†], Z. Chen[1], Y. Q. Zong[1] and W. Zeng[4]

[1]*State Key Laboratory of advanced Design and Manufacturing for Vehicle Body, Hunan University, Changsha 410082, P.R. China*
[2]*Hunan Institute of Science and Technology, Yueyang, 414006, P.R. China*
[3]*Hunan University of Arts and Science, Changde 415000, P.R. China*
[4]*CEAS-Biomedical Engineering, University of Cincinnati, 2901 Woodside Dr., Cincinnati, OH 45221, USA*

†*Corresponding Author Email: htm426@hnu.edu.cn*

(Received July 19, 2015; accepted March 2, 2016)

ABSTRACT

In order to study the aerodynamic responses of a vehicle pitching around its front wheel axle, large eddy simulation (LES) is used to investigate the flow-field around road vehicle. The numerical method is validated by 1/3-scale wind tunnel model on steady state. The LES results keep good agreement with the wind tunnel data. Furthermore, LES is applied to simulate the sinusoidal-pitching motion of vehicle body with frequency 10Hz. It can be found that the aerodynamic force coefficient and flow field changed periodically when the vehicle body takes periodically motion, whose results are completely different from the quasi-steady simulation results. When vehicle body suddenly changes direction, the hysteresis effects of the flow is clearly shown through investigating the transient flow field, aerodynamics force coefficient and pressure coefficient. The hysteresis effects of the transient flow field is also studied by vortices visualization technical, and the transient flow field from space and time is further understood.

Keywords: LES; Pitching motion; Vortices; Transient aerodynamics; Hysteresis effects.

NOMENCLATURE

Cs	model coefficient	W	width
Cd	drag force coefficient		
Cl	lift force coefficient	u_i	the *i*th velocity component
Cp	pressure coefficient	u^*	wall friction velocity
H	height	y^+	wall normal distance
L	length	θ	pitching angle
P	pressure	β	circumferential angle
P_t	static pressure	ρ	air density
P_∞	reference pressure	v	kinematic viscosity
Re	Reynolds number	y^+	wall normal distance
S_{ij}	strain rate tensor	f_d	Van Driest damping function
U_∞	wind speed	f	frequency
		Δ	filter width

1. INTRODUCTION

For a long time, vehicle aerodynamic performances is evaluated by steady-state method. For example, adopting discontinuous change angle to conduct simulation or experiment, the result is obtained for one position at a time, which can be called as quasi-steady method (Baker 2010). Actually, vehicle will be affected by environmental factors (Darling *et al*. 2003; Valerie *et al*. 2014), own state (Hrvoje *et al*. 2014; Rocchi *et al*. 2012), etc., which leads to the transient change process of the flow field. The transient flow field could cause handling, stability and performance issues (Joshua *et al*. 2013).

Considering the importance of the transient aerodynamics, numerous researchers have carried out wind tunnel experiments (Passmore *et al*. 2001; Zhu *et al*. 2010) or adopted advanced test methods (Lichtneger *et al*. 2015; Volpe *et al*. 2014) to evaluate it. Using experiment or adopting advanced test

method to study the transient aerodynamic is very complicated and time-consuming, and sometime it is cost and unable to find the reasonable solutions. On the other hand, the computational fluid dynamics (CFD) method becomes a very effective method to analyze transient aerodynamic in the past several decades. It can provide enough information of transient response and investigate the aerodynamic force of vehicles when driving on roads. Therefore, more and more researchers used CFD method to study transient aerodynamic in recent years. The RANS and LES methods are used very wide in vehicle aerodynamic at present. However, the traditional RANS method isn't appropriate for transient analysis, especially when the vehicle is driving on complex condition. For example, Guilmineau (2008) presented that using the RANS method to simulate unstable flow field in a complex condition was seldom successful. However, LES has been successfully applied in number of unsteady wake analyses of vehicle body. Tsubokura *et al*. (2010) used LES to investigate the vehicle in transient crosswinds, and the results of aerodynamic forces and moments showed good consistent with the experimental. Krajnovic (2014) used LES to study the drag reduction of an Ahmed body, which also showed good consistent with the experiments. However, the studies mentioned above mainly focus on the influence of the crosswind and environment, and only few refers to the influence of the vehicle's own state.

Due to the roughness of the road or driver's operations, a moving vehicle on the road often suffers from pitching motion. The pitching motion of the vehicle could lead to vehicle stability problem. Moreover, with the promotion in engine power and better road condition have supported higher driving speed, more severe consequences could be appeared because its effect on the drive control, comfort and safety. While only a few researches can be found on the aerodynamics of the pitching motion of vehicle body so far. Aschwanden *et al*. (2008) used the wind tunnel to study the ride height change of the race cars, and found that the motion aerodynamic caused greater effects on the simplified race car model in the simulated movement. Cheng *et al*. (2013) studied the influence of different combinations of A, C pillar to the aerodynamic stability of the vehicle, and found the importance of the proper shaping of A-pillar and C-pillar to control the vehicle body pitching oscillation. However, their researches mainly focused on transient aerodynamics force to the stability of vehicle, the mechanism of the transient flow field has not been studied yet. In a real vehicle, the vehicle body is very complicated due to many small parts. The flow structure produced by these small parts can interplay with each other and hinder to deeply investigate. Therefore, an important purpose of this paper is to study the results between transient and quasi-steady state, and the mechanisms involved in physical will be investigated and explained.

Cheng *et al*. (2012) introduced the aerodynamic-damping coefficient to evaluation vehicle's stability in pitching motion. They found that quasi-steady analysis in pitching motion was not sufficient because of the hysteresis effects. However, the hysteresis and phase shift in the process of pitching oscillation was not fully considered. Some researchers have studied the hysteresis and phase shift, but the most of them used some simplified models, such as the bluff-body, Ahmed model and so on. For example, Krajnovic (2011) simulated the oscillation of bluff-body model around its vertical axis, and found the hysteresis and phase-shift phenomenon in the dynamic flow condition. David *et al*. (2013) employed a simple sharped-edge rectangular to study flow around a four vehicle in row, and found that the longitudinal oscillations of a platoon member would produce hysteresis effects of the drag force coefficient of neighbor members. The researches of hysteresis and phase shift mentioned above all occurred during vehicles driving in condition of crosswind or suffering yawing motion, but the situation of vehicle's pitching motion is seldom studied. The models used by the researchers are very simplified, which can't reflect the intricate detail of the vehicle. Besides, the flow field around the vehicle can't be truly demonstrated. An important purpose of this paper will study the hysteresis of the flow around the pitching body via a full vehicle model with true geometry, which is able to provide enough information of transient flow with high-fidelity in time and space.

The paper is organized as follows. Numerical set-up, vehicle model and experimental are presented in second section. The results are presented and discussed in third section. Finally, the fourth section is the conclusion.

2. NUMERICAL SET-UP

2.1 Governing Equations and Discretization

The governing equations of LES are the incompressible Navier–Stokes：

$$\frac{\partial \overline{u}_i}{\partial x_i} = 0 \tag{1}$$

$$\frac{\partial \overline{\mathrm{u}}_\mathrm{i}}{\partial t} + \frac{\partial}{\partial x_\mathrm{j}} \overline{\mathrm{u}}_\mathrm{i} \overline{\mathrm{u}}_\mathrm{j} = -\frac{\partial \overline{\mathrm{P}}}{\partial x_\mathrm{i}} + 2\frac{\partial}{\partial x_\mathrm{j}} (\nu + \nu_{\mathrm{SGS}}) \ \overline{\mathrm{S}}_{\mathrm{ij}} \tag{2}$$

$$\overline{P} = \frac{p}{\rho} + \frac{\overline{u_i u_j} - \overline{u}_i \overline{u}_j}{3} \tag{3}$$

where u_i is the ith velocity component, p stands for the pressure, ρ denotes the density and v represents the kinematic viscosity of the fluid. Where S_{ij} corresponds to the strain rate tensor, defined as

$$\overline{S}_{\mathrm{ij}} = \frac{1}{2}\left(\frac{\partial \overline{u}_j}{\partial x_i} + \frac{\partial \overline{u}_i}{\partial x_j}\right) \tag{4}$$

Where the ν_{SGS} in Eq. (2) represents the effect of sub-grid-scale (SGS) turbulence. The standard Smagorinsky model is adopted, and the ν_{SGS} is modeled as

$$\nu_{SGS} = (C_s f_d \Delta)^2 \sqrt{2\overline{S}_{ij}\overline{S}_{ij}} \tag{5}$$

where C_s represents the model coefficient, and the value of C_s is 0.1 which used in many similar types studies(Osth and Krajnovic 2014). Δ represents the filter width, and f_d represents the Van Driest damping function, which is defined as

$$f_d = 1 - \exp\frac{-y^+}{25} \tag{6}$$

where y^+ is the wall normal distance.

2.2 Numerical Method

The incompressible equations (1) and (2) are discretized using the commercial finite volume solver ANSYS Fluent 14.0. The discretization is done by a collocated grid arrangement. A second-order conservative scheme is used to approximate the convective fluxes, for the spatial derivative, and blending with the first-order upwind scheme to avoid numerical oscillation (Verstappen *et al*. 2002). The diffusive terms containing viscous plus sub-grid terms are approximated by a central differencing interpolation of second-order accuracy (Trias *et al*. 2011). The time marching procedure is done using the implicit second-order accurate three-time level scheme. The pressure-velocity coupling is solved by simple scheme.

2.3 Description of the Vehicle Model

In Fig. 1, the vehicle model is shown in four different views. The rear view mirror and door handle are ignored, and the underfloor is simplified as a plane. In order to compare with the wind tunnel experiment, a 1/3-scale model is adopted. The overall length, width and height of the model is 1588mm, 642mm, and 505mm, respectively. The length of the wheel base is 952mm, and the length of the front overhang and rear overhang is 290mm and 346mm, respectively. The coordinate of the point P1 and P2 is (1407, 0, 283) and (1521, 0, 196). The clearance between the rear tire and the rear wheel arc is 72mm. The origin of the coordinate in x, y, z direction is at the forefront, lowest, and center of symmetry of the vehicle body, as shown in Fig 1.

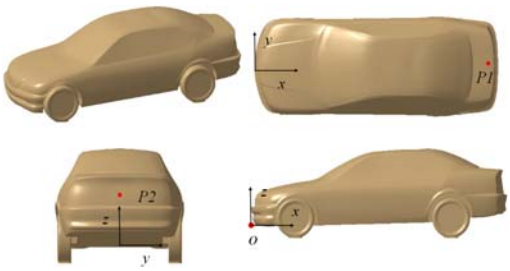

Fig. 1. Simplified vehicle model and the Cp monitor point.

2.4 Computational Domain and Boundary Conditions

The computational domain is presented in Fig. 2. The cross section covers with 4W on both side and 7.2H from the roof to the floor. The blockage ratio in this paper is less than 1.2%, which is better than the typically accepted range of 5% in wind tunnel test (Tsuei *et al*. 2001). A uniform and in time constant velocity profile U_∞ =30m/s is applied on the inlet, which is equivalent to those adopted in the experiment. The Reynolds number, based on the inlet velocity and vehicle length, and Re is 3.26×10^6. The upstream turbulence intensity is 0.5%. Pressure-outlet boundary is used on the outlet. In order to avoid the formation of boundary-layer, the floor is divided into two parts. Five vehicle length from the inlet boundary to the model on the floor is the part one and is defined as free slip wall, whose purpose is to simulate the effect of suction floor in wind tunnel test. The other part of the floor and vehicle surface are set as no-slip wall boundary. The roof and side wall are set as free-slip wall boundary (shown in Fig. 2(a)).

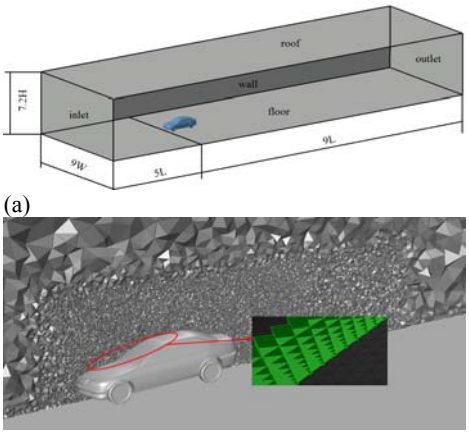

(a)

(b)

Fig. 2. a)computatinal domain; b)grid topology.

2.5 Computational Grid and Grid Independence Test

The flow field over road vehicle is very complex, and the vortices around the vehicle at the position behind 1.5L in the rear of the vehicle begin to settle down (Fuller *et al*. 2014). Therefore, the grid topology is divided into several blocks in this paper to capture more details of flow information around the vehicle and save the computing resources as shown in Fig. 2(b). The finest block is the boundary layers region, which is generated from the vehicle's surface with 10 prism layers, with a growth rate of 1.15. The mean $y^+=u^*n/\upsilon$, where u^* stands for the wall friction velocity, and n is the distance from the center of the first cell to the vehicle wall, and υ stands for the kinematic viscosity of air. The average y^+ is around 1.0 in this study. Near to the boundary layers is the second-finest block, which is intended to capture more detail information about the flow field around the vehicle. The coarse mesh used in other regions is to improve the computational efficiency. The ANSYS ICEM-CFD is used to generate the unstructured meshes.

The number of cells affect the calculated results, so grid independence test (Alamaan *et al*. 2014) is performed. The criteria for selecting the number of

Table 1 Detailed grid size tests and experiment

Data	Case 1	Case 2	Case 3	Case 4	Case 5	experiment
Number of cells	21604882	19916966	18090813	16126342	14909653	
Cd	0.285	0.285	0.287	0.291	0.296	0.284
Cl	-0.048	-0.048	-0.051	-0.055	-0.060	-0.047

cells is based on the Cd and Cl. Cd represents the aerodynamic drag force coefficient and Cl represents the aerodynamic lift force coefficient. The simulation results are compared to experimental data when vehicle body is at the horizontal position (θ=0deg) as shown in Table 1. The detail information of the experiment will be introduced in next subsection. According to the simulation and experiment results, and considering a large amount of computing resources and time required for the simulation in this study, the case 2 is chosen.

2.6 Validation

In order to validate the accuracy of the simulation by LES method, the steady experiment is conducted in the HD-2 boundary layer wind tunnel at Hunan University. The length of automotive test section is 17m and its cross sectional area is 3*2.5m. The maximum wind speeds is 58 m/s and the maximum power of propeller is up to 617kW. The average turbulence intensity is about 0.13%. In order to ensure the accuracy of the experiment, a 1/3-scale model is used in the experiment as shown in Fig 3(a). The wind velocity and vehicle model dimension is consistent with those in simulation.

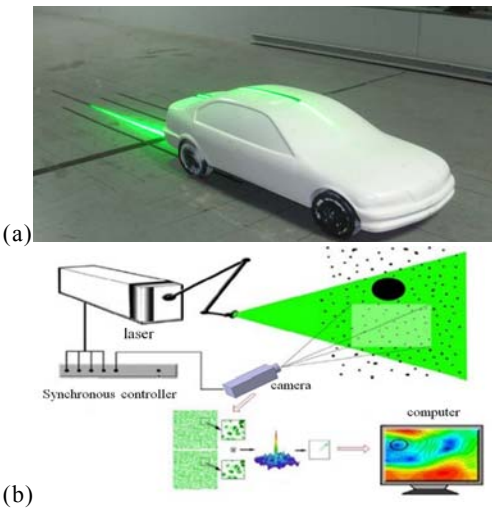

Fig. 3. a) vehicle in wind tunnel. b) sketch of PIV working.

The Particle Image Velocimetry (PIV) system is used to measure the wake on the section of Y=0 as shown in Fig 3. The PIV is placed on the top of the test section of wind tunnel, with 500*mJ/pulse* pulse energy and with green light of wavelength 532*nm* used for illuminating and tracking the particles in the flow field, a data acquisition system and a CCD camera with 5H*z* frame-rate and 4000*2672 pixels.

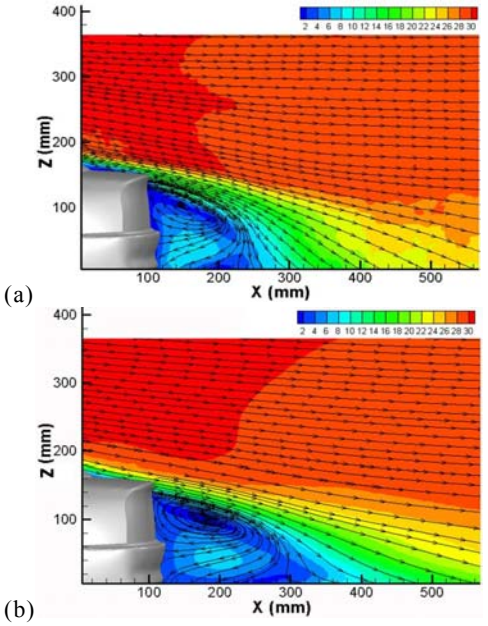

Fig. 4. Comparison of velocity contours and the velocity streamlines between wind-tunnel measurement and simulation on Y=0 section. a) experiment; b) simulation.

From Table 1, it can be found that the results of experiment and simulation obtained from case 2 with a deviation of *Cd* is near to 0.4%, and the deviation of *Cl* is near to 2.2%. The deviation of aerodynamic force coefficient between the experiment and simulation in the field of automotive aerodynamics could be accepted. Fig 4 shows the comparisons of the velocity contours and the velocity streamlines of the experiment and simulation on the section of Y=0 at the tail of the vehicle. Both of them have a pair of opposite revolving vortex, and the speed of the vortices is reduced to vortex core, which leads to a recirculation zone. The vortices structures are similar in the recirculation zone. The height of vortices is the same in Z-direction, which are at the region from Z=60mm to Z=140mm. The length of the vortices have a slight difference in x-direction. The vortices obtained from experiment is at the region from x=100mm to x=200mm, and the vortices obtained from simulation is at the region from x=100mm to x=250mm. The vortex of the simulation slightly longer than the experimental, which

may be induced by the subtle inconsistent between they are. This clearly demonstrates the effective and feasibility of LES using high-fidelity simulations.

2.7 Forced Pitching Motion Condition

Okada et al. (2009) reported that the influence of the fluctuation at rear-end is bigger than that at the front. Therefore, when the transient simulation is taken in this paper, the vehicle body is rotating to a lateral axis, and the axis is located at the front wheel axle as shown in Fig 5(a). The dynamic mesh is used to achieve the vehicle body pitching motion in ANSYS Fluent 14.0. The vehicle and the boundary layer is the dynamic zone, and the type is set as rigid body. Two types of meshing methods smoothing and remeshing are used in this study. The motion setting is similar to the test of Okada at al. The motion is defined as

$$\theta = -\theta_1 \sin\phi(\mathrm{t})$$

where θ_1 equal to 2deg. Although this value is bigger than the value of actual situation, it is better to reproduce pitching motion process. While $\phi(t) = 2\pi ft$, the frequency f is 10Hz and the pitching motion periodic time is 0.1s as shown in Fig 5(b). The time step size is 0.00005s.The phase-averaged results reported in this paper is computed over 10 periods after LES achieve stable periodic state. The simulation time (32CPU and 128G memory) is approximate to 300 hours.

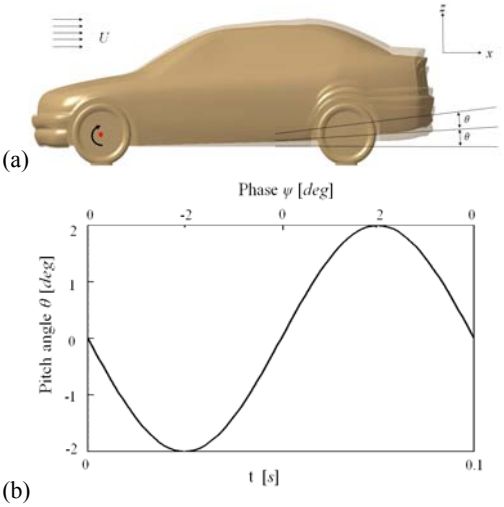

Fig. 5. a) conventions of pitching motion. b) conventions of pitching angle

3. RESULTS AND DISCUSSION

3.1 Transient Effects on Aerodynamic Force coefficient Due to Pitching Motion

The aerodynamic force coefficient is saved at each time step as shown in Fig 6 and Fig 7. Fig 6(a) and Fig 7(a) show that the change trend of the quasi-steady simulation results is consistent to the steady experiment results. Because the quasi-steady method is realized by steady simulation, the deviation of the two cases are very small.

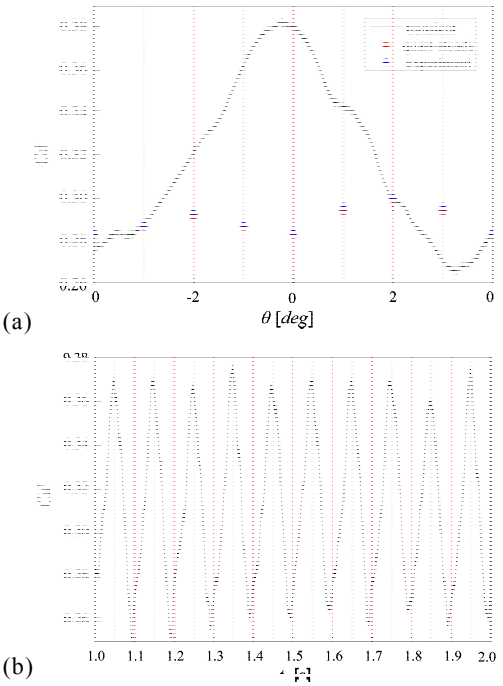

Fig. 6. a) periodic in *Cd* and b) time history of *Cd* obtained from LES simulation.

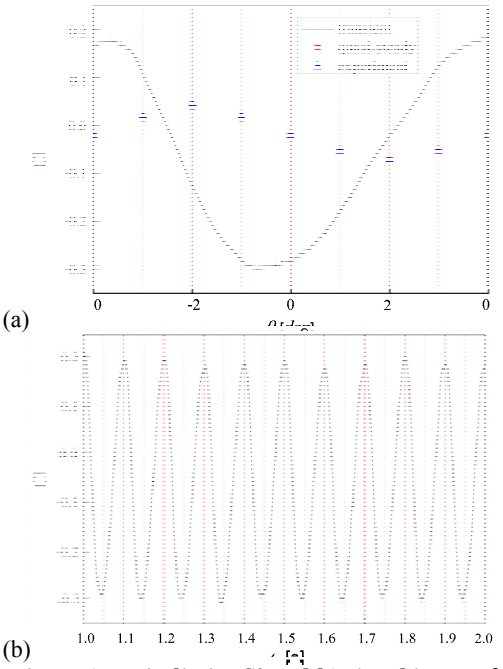

Fig. 7. a) periodic in *Cl* and b) time history of *Cl* obtained from LES simulation.

When the vehicle body takes periodically pitching motion, Cd and Cl also changes periodically as shown in Fig 6 and Fig 7, respectively. Although the change of amplitude is very small when the vehicle body

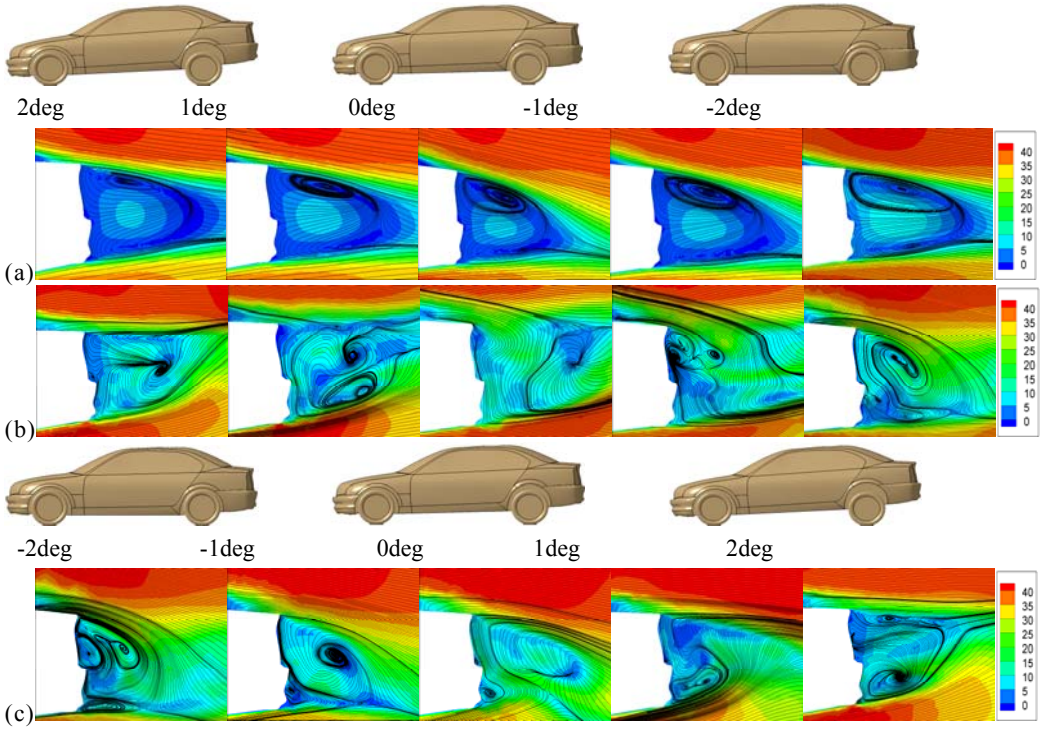

Fig. 8. Streamline project on the section y=0: (a) quasi-steady simulation, (b) and (c) transient simulation.

takes periodically pitching motion, the effect on the aerodynamic force coefficient can't be ignored. The flow field around the vehicle will have transient change, which will have transient effect on the aerodynamic force coefficient. Fig 6 and 7 present the change rule of aerodynamic force coefficient is completely different between transient and quasi-steady simulation state. For example, the position and value of the maximum and minimum aerodynamic force coefficient on the transient simulation state are quite different from the quasi-steady state and experiment. On the transient simulation state the maximum drag force coefficient appears near to the position θ=0deg (the vehicle body moves from -2deg to 2deg). The maximum value is 0.383. The minimum drag force coefficient appears near to the position θ=0deg (the vehicle body moves from 2deg to -2deg). The minimum value is 0.265. For quasi-steady simulation, the Cd also shows the periodic changes. However, the results of quasi-steady and transient simulation are quite different as shown in Fig 6(a). The minimum value appears at the position θ=0deg, with the minimum value 0.284. As the vehicle body leaving the position θ=0deg, the drag force coefficient gradually increases. The maximum appears at the position θ=2deg, and the maximum value is 0.301. The Cl also changes periodically along with the vehicle body periodic pitching motion as shown in Fig 7(a) and 7(b), but it would not be introduced in details at here. From the results could be found that the maximum value of transient drag force coefficient is about 1.4 times of quasi-steady, and the maximum value of transient lift force coefficient is about 1.6 times of quasi-steady.

Fig 8 presents the evolution of the velocity streamline on the section Y=0 during the sweep on quasi-steady and transient simulation state. In Fig 8(a), the velocity streamline on quasi-steady state has a little difference in the position of the vortices and the size at the five different position. The main reason of this phenomenon is that the flow field around the vehicle is not influenced by the transient effect of the vehicle body pitching motion. However, the flow field around the vehicle body is influenced by the transient effect of the vehicle body pitching motion on transient simulation state, which leads to the difference of the velocity streamline on different position as shown in Fig 8(b) and Fig 8(c). The wake flow field of vehicle is very important to the aerodynamic force coefficient (Aljure et al. 2014), and the wake flow field is quite different at quasi-steady and transient simulation state. Therefore, the aerodynamic force coefficient is quiet different between the transient simulation state and the quasi-steady state. From the results of the aerodynamic force coefficient and the flow field, it could be found that quasi-steady simulation is not able to reflect the actual condition, but the transient simulation is an important method to reflect the vehicle aerodynamics in actual condition.

From Fig 6 and Fig 7 could be found that a small pitching angle of vehicle body will lead to the aerodynamic force coefficient changing

obviously at the extreme position. The major reason for the changing is the hysteresis effects of the flow field. The hysteresis phenomenon will be discussed in next subsection.

3.2 Time-averaged pressure

The time-averaged pressure distribution is used to calculate the local pressure coefficient (Cp). The Cp is defined as

$$C_p = 2((p)_t - p_\infty)/\rho U_\infty^2$$

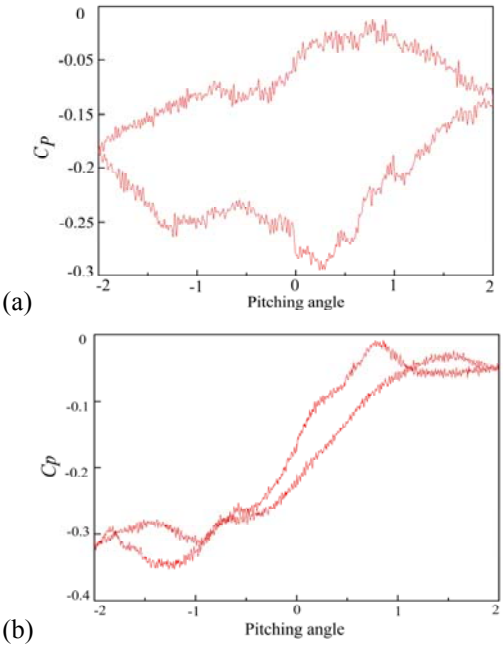

Fig. 9. Cp value at different point. a) P1. b) P2.

Figure 9 shows the evolution of Cp at point P1 and P2 during the entire oscillating sweep of the vehicle. Since the phase change of the rear end is bigger than the front end in this study, the point P1 and P2 are chosen at the rear end. Cheng *et al*. (2012) reported that the trunk deck contribution accounts for the pitching-stability. Therefore, the point P1 and P2 are set on the trunk deck. Considering of the typical flow field at the rear of vehicle, the point P1 is on the upper surface of truck lid, and point P2 is on the rear surface of trunk lid as shown in Fig 1. The coordinate of the point P1 and P2 is (1407, 0, 283) and (1521, 0, 196), respectively. It could be found that the sensitivity to pitching motion is very different for the two points. This is because the flow field behind the trunk is more complex than upper of the trunk (Wang *et al*. 2014; Mestiri *et al*. 2014). Fig 8 can be used to explain this phenomenon. Fig 8 presents that the wake flow field is quite different when vehicle body is at different positions, which leads to the difference of the Cp. At the extreme position θ=-2 and θ=2, Cp don't immediately change when vehicle body change moving direction, but Cp is experienced with a certain delay in time. The aerodynamic force coefficient also have similar phenomenon as shown in Fig 6(a) and 7(a). From above can be found that between two halves of the sweep, each sweep can produce unique data. The change rule of aerodynamic force coefficient and Cp illustrates that there is a hysteresis phenomenon when vehicle body takes pitching motion. The hysteresis phenomenon will be discussed in next subsection.

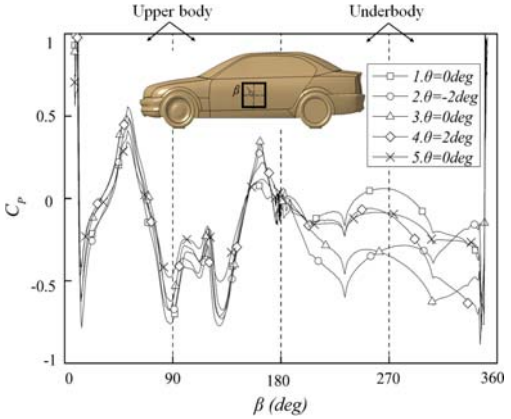

Fig. 10. Cp distributions at Y=0 section, (1)-(4) transient state, (1).the vehicle body moves from 2deg to -2deg, (3).the vehicle body moves from -2deg to 2deg). (5) quasi-steady state.

Figure 10 shows Cp at the y=0 section. The Cp plot along the circumferential angle (β), and measured clockwise around an axis. The axis pass through the weight center of the vehicle and zero angle is aligned with the horizontal axis. It is quite different for the change rule of Cp between the transient and quasi-steady simulations. The difference of Cp between transient and quasi-steady simulation is very small on the upper vehicle body from the front bumper to the front of the roof. However, there is a big difference from rear of the roof to the trunk-lid, especially for the minimum value. The value of Cp on the transient simulation state is smaller than Cp on quasi-steady simulation state.

The change of Cp is very small from the upper of the front bumper to the rear windshield on the transient simulation state as shown in Fig 10. However, a large variation of Cp appears from the upper of trubk-lid to the underbody, for example, the difference of Cp reach to 0.5 at the same position on the vehicle body on different state. The main reasons to the change of Cp are included as following,

1. Compared to the front end, the phase change of the rear end is larger. Which leads to a more obviously affect on the flow field around the vehicle body.

2. The nature of the surrounding fluid and the inertia effects leads to the wake vortex separation at different states.

3. The change of the space between the underbody and the floor lead to the change of velocity and

direction of the flow around the vehicle body.

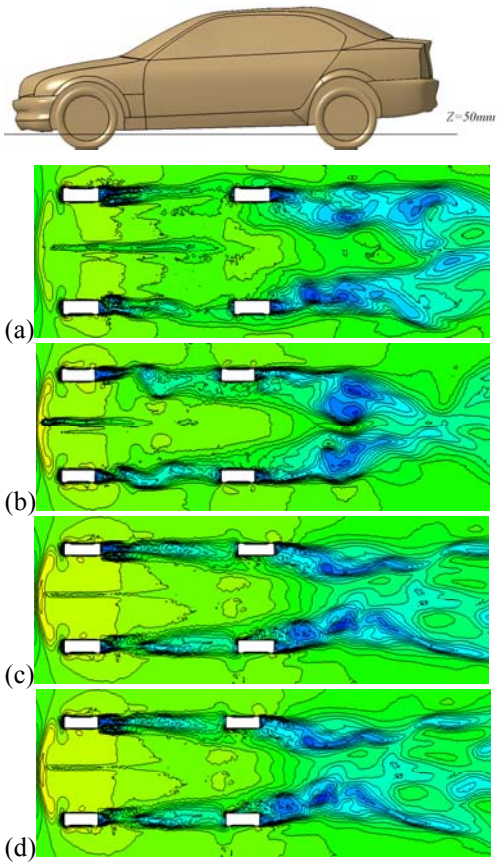

Fig. 11. Flow Velocity under the vehicle on XY-section (z=50mm) at different positions (a) θ=0deg (the vehicle body moves from -2deg to 2deg) (b) θ=-2deg (c) θ=0deg (the vehicle body moves from -2deg to 2deg) (d) θ=2deg.

Flow velocity under the vehicle on XY-section at 50 mm above the ground when vehicle body at different positions is visualized in Fig 11. The change of space between the underbody and the floor is not consistent when the vehicle body takes pitching motion, which is due to the fact that the vehicle body rotates to the center of front axle. It leads to the flow velocity quite different at the same section when the vehicle body is at different positions. For example, at the same position θ=0deg as shown in Fig 11(a) and Fig 11(c), the flow velocity around the vehicle is also quite different when vehicle body comes from different directions, which leads to the difference of Cp on the section of Y=0 and aerodynamic force coefficient at the position θ=0deg.

3.3 Hysteresis Phenomena and Phase Shift

Figure 12 presents the instantaneous flow structure around the vehicle in the side view. Several authors have proposed methods for identifying coherent structures of the flow (Hunt *et al*. 1998; Jeong *et al*. 1995). In this work the Q-criterion proposed by Hunt *et al*. (1998) is chosen for the identification of the coherent structures, Q is defined as:

$$Q = -(\partial\overline{u}_i \partial\overline{u}_j) / (2\partial x_i \partial x_j)$$

In Fig 6, Fig7, Fig 9, and Fig 12, the hysteresis effects can be observed obviously when the vehicle body sweeps between the extreme position θ=-2deg and θ=2deg. Because of the hysteresis effects, the Cp distribution and the aerodynamic force coefficient are different when vehicle body moves toward the same position from different direction. It will lead to larger difference due to a small pitching angle. Fig 9 presents that when the position of the vehicle body changed, the flow field around the vehicle is influenced by the hysteresis effects, which lead to a phase shift of Cp on the vehicle body. Fig 12 indicates that the surrounding flow tries to follow up when the vehicle body takes pitching motion, but there is a lag time due to the nature of the surrounding fluid and the inertia effects of the flow, which lead to the response of the flow around the vehicle body.

Because of the lag time of the around flow, a phase shift phenomenon could be found in Fig 6, 7 and 9. The phase shift appears at both halves of the sweep when the vehicle body takes pitching motion. Due to the existence of the phase shift, the vortices and other data on quasi-steady and transient simulation state are quite different. Fig 12 shows that the surrounding flow tries to follow up when the vehicle body takes pitching motion. But there is a big difference of the flow around the vehicle body at the same position at different simulation state as shown in Fig 13 and Fig 14.

The important observation from Fig 12 and Fig 13 is that the surrounding flow has some difference at the same position if the vehicle body's rotation is in the direction of the increasing or decreasing pitching angles. Fig 13 shows the flow at the extreme position θ=2deg and θ=-2deg. When the vehicle body reaches the extreme position and starts to change direction, the nature of the surrounding fluids and the inertia effects of the flow accelerate the vortices structure to change. Fig 13 (b) and Fig 13 (c) show that the length, height and shape of the vortices are different when the vehicle body reaches and then leaves the position θ=-2deg. However, Fig 8(b) and Fig 8(c) reveal that the change of moving direction of the vehicle body will lead to the bottom change of space, and rail velocity. When the vehicle body reaches to position θ=-2deg, the velocity at the tail is smaller than departure. Which leads to the negative pressure zone closer to the body, and then the intensity of the rise vortices will be reduced. Because of the influence of the nature of the surrounding fluids, the vortices direction keep the trend of upper stage when the vehicle body depart the position. A similar phenomenon could be observed at the position θ=2deg, as shown in Fig 13 (e) and Fig 13 (f). Such great change is exposed in Fig 12 and Fig 13 by quite different sizes and positions of the flow structures in the wake. As the flow structures in the wake changed, it could lead to the change of pressure on vehicle body, and

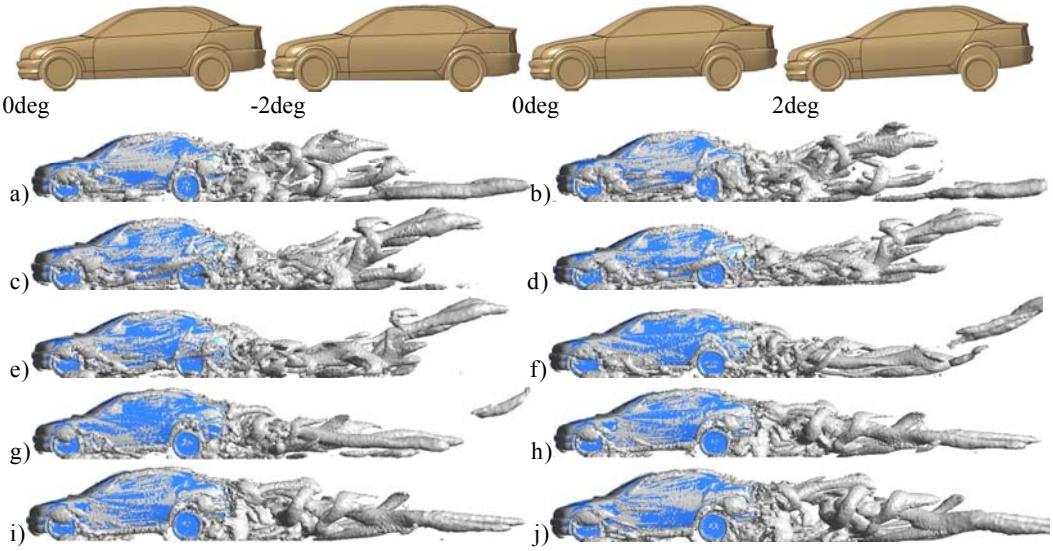

Fig. 12. Iso-surface of the second invariant of the velocity gradient tensor Q=20 000. a) θ=0deg,b) θ=-1deg, c) reach to θ=-2deg, d) leave θ=-2deg, e) θ=-1deg, f) θ=0deg, g) θ=1deg, h)reach to θ=2deg, i) leave θ=2deg, j) θ=1deg.

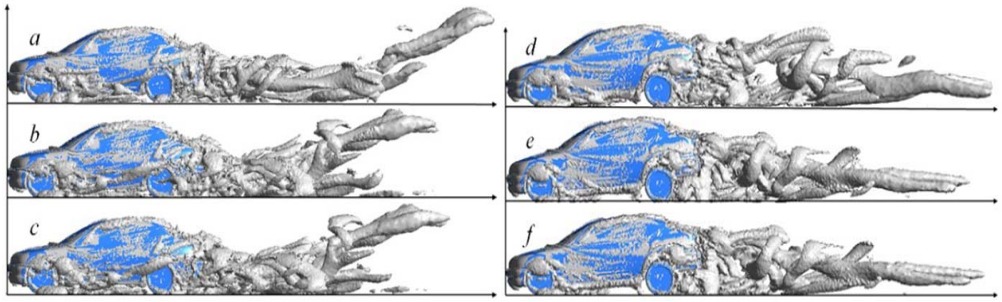

i) the position θ=-2deg ii) the position θ=2deg

Fig. 13. Iso-surface of the second invariant of the velocity gradient tensor Q=20 000 for position θ=-2deg and θ=2deg. (a), (d) quasi-steady, (b), (c), (e), (f) transient.

the pressure on vehicle body has an important influence on the aerodynamic force coefficient.

Figures 13 and 14 present some changes in the body surrounding flow field structure on quasi-steady and transient simulation state. While Fig 13(i) and 13(ii) show the vortices structures at the two different simulation state are quite different when the vehicle body at the extreme position θ=-2deg and θ=2deg. The change tendency of vortices in transient simulation state is similar, but there are some differences. The flow around the vehicle body has no time to adjust the sudden change in the direction of pitching, which leads to this difference. Fig 14(b) shows that the vehicle body changes the direction from 0deg to -2deg, and Fig 14(c) shows the vehicle body changes direction from -2deg to 0deg, while the vortices are completely different. Although in Fig 14(c) the wake flow is probably still influenced by the rotation of the body from 0deg to -2deg, the influence of the wake flow from the rotation direction from -2deg to 0deg is bigger, and the wake adjust the direction of rotation.

Figure 8 shows that the streamline is quite different at some position when vehicle move from differect direction. For example, at the position of θ=-1deg, there is upward trends of the streamline at the bottom when vehicle body moves from 0deg to -2deg. While there is downward trends of the upper streamline when vehicle body moves from -2deg to 0deg. Similar phenomenon in vortices can be found at the position θ=1deg. However, this phenomenon is not at the extreme position θ=-2deg and θ=2deg.

It should be noted that only one type of pitching amplitude and frequency is studied in this paper. While the vehicle driving on the road will encounter various amplitudes and frequencies, and it is worthwhile to study how the aerodynamic force coefficient is influenced by the change of amplitude and frequency. Moreover, only one type of velocity is considered in this study, further investigations of the effect of high speed on vehicle stability can be study in future.

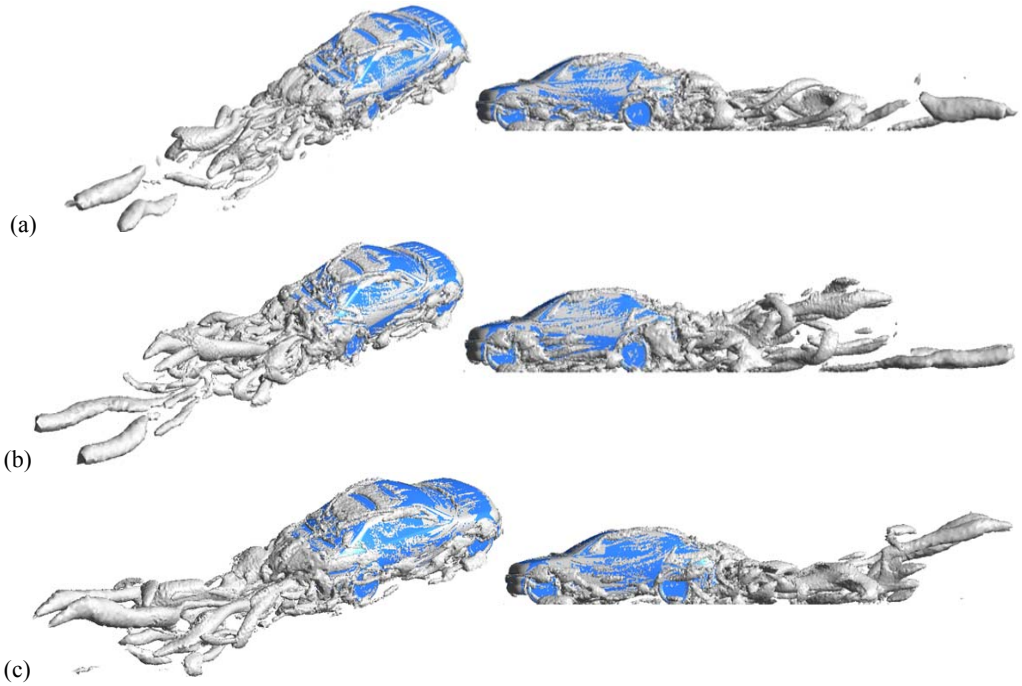

Fig. 14. Iso-surface of the second invariant of the velocity gradient tensor Q=20 000 for position θ=-1deg. a) quasi-steady. b）transient flow for decreasing -1deg. c) transient flow for increasing -1deg.

4. CONCLUSION

In the present studies, LES is used to simulate the vehicle body pitching motion. The feasibility of LES is validated by the wind tunnel experiments. Large difference could be found between the transient simulation results and quasi-steady simulation results. The maximum value of transient drag force coefficient is about 1.4 times than quasi-steady drag force coefficient, and the maximum value of transient lift force coefficient is about 1.6 times than quasi-steady lift force coefficient. The change of the pressure on the underbody on the transient simulation state is larger than other parts, which have greater contribution to the aerodynamic force coefficient. Moreover, LES provides enough information which the wind tunnel experiment and RANS simulation are difficult to give. These information can help to explain the change of aerodynamic force coefficient and Cp, the hysteresis and phase shift. It shows that LES is an important method for the assessment of vehicle aerodynamics.

When the vehicle body takes pitching motion, except the space between the underbody and the floor, which could influence the aerodynamic force coefficient. There is another important influence factor which is the memory effects of the flow and the inertia of the flow. Furthermore, through the vortices visualization techniques, and the change of rule Cp on the special point can be found that each sweep generates unique flow field, because of the impact of the hysteresis effects.

ACKNOWLEDGMENTS

This work is supported by Key Project in the Science and Technology Program of Changsha, China (K1501011-11), National Automotive High Level Independent Innovation Program of China, National Hundred, Thousand, and Ten Thousand Talent Program of Ministry of Transport of China (Grant No.20120222), Independent Subject of State Key Laboratory of China (Grant No.734215002), and Innovation Team of Ministry of Finance of China (Grant No.04200036017), National Natural Science Foundation of China (Grant No. 51305312).

REFERENCES

Alamaan, A., A. Ashraf and A. Waqar (2014). Passive drag reduction of square back road vehicles. *J. Wind Eng. Ind. Aerodyn.* 134, 30-43.

Aljure, D. E., O. Lehmkuhl, I. Rodriguez and A. Oliva (2014). Flow and turbulent structures around simplified car model. *Comput Fluids* 96, 122-135.

Aschwanden, P and J. Muller (2008). The Influence of Motion Aerodynamics on the Simulation of Vehicle Dynamics. *SAE Paper* 2008-01-657.

Baker C. J. (2010). The simulation of unsteady aerodynamic cross wind forces on trains. *J. Wind Eng. Ind. Aerodyn.* 98, 88–99.

Cheng, S. Y, M. Tsubokura, T. Nakashima, Y.

Okada and T. Nouzawa (2012). Numerical quantification of aerodynamic damping on pitching of vehicle-inspired bluff body. *J. Fluids Struct* 30, 188-204.

Cheng, S. Y., M. Tsubokura, Y. Okada, T. Nouzawa, T. Nakashima and D. H. Doh (2013). Aerodynamic stability of road vehicles in dynamic pitching motion. *J. Wind Eng. Ind. Aerodyn.* 122,146-156.

Darling, J. and P. M. Standen (2003). A study of caravan unsteady aerodynamics. P I Mech. Eng. D-J AUT 217,551-560.

David, U. and S. Krajnovic (2013). LES of the flow around several cuboids in a row. *Int. J. Heat Fluid Flow* 44, 414-424.

Fuller, J. and M. A. Passmore (2014). The importance of rear pillar geometry on fastback wake structures. *J. Wind Eng. Ind. Aerodyn* 125, 111-120.

Guilmineau, E. (2008). Computational study of flow around a simplified car body. *J. Wind Eng. Ind. Aerodyn.* 96, 1207–1217.

Hrvoje, K., P. Lorenzo, B. Alessandra and G. Bartoli (2014). Optimizing height and porosity of roadway wind barriers for viaducts and bridges. *Eng. Struct* 81, 49-61.

Hunt, J, A. Wray and P. Moin (1998). Eddies, stream and convergence zones in turbulent flows [M]. Tech. Rep. CTR-S88, Center for turbulent research.

Jeong, J. and H. Fazle (1995). On the identification of a vortex. *J. Fluids Mech.* 285, 69-94.

Joshua, F., B. Matt, G. Nikhil and *et al*. (2013). The importance of unsteady aerodynamics to road vehicle dynamics. *J. Wind Eng. Ind. Aerodyn.* 117, 1-10.

Krajnovic, S (2014). Large Eddy Simulation Exploration of Passive Flow Control around an Ahmed Body. *J FLUID ENG-T ASME* 136, 1-10.

Krajnovic, S. (2011). Large Eddy Simulation Investigation of the Hysteresis Effects in the Flow around an Oscillating Ground Vehicle. *ASME: J. Fluids Eng.* 133(12), 1-9.

Lichtneger, P. and B. Ruck (2015). Full scale experiments on vehicles induced transient loads on roadside plates. *J. Wind Eng. Ind. Aerodyn.* 136, 73–81.

Mestiri, R., A. Bensoltane, L. Keirsbulck, F. Aloui and L. Labraga (2014). Active Flow Control at the Rear End of a Generic Car Model Using Steady Blowing. *J APPL FLUID MECH* 7(4), 565-571.

Okada, Y., T. Nouzawa, T. Nakamura and S. Okamoto (2009). Flow Structures above the Trunk Deck of Sedan-Type Vehicles and Their Influence on High-Speed Vehicle Stability 1st Report: On-Road and Wind-Tunnel Studies on Unsteady Flow Characteristics that Stabilize Vehicle Behavior. *SAE Paper*. 2009-01-0004.

Osth, J. and S. Krajnovic (2014). A study of the aerodynamics of a generic container freight wagon using Large-Eddy Simulation. *J. Fluids Struct* 44, 31-51.

Passmore, M. A, S. Richardson and A. Imam (2001). An experimental study of unsteady vehicle aerodynamics. *P I Mech. Eng. D-J AUT. 215*, 779–788.

Rocchi, D., L. Rosa, E. Sabbioni, M. Sbrosi and M. Belloli (2012). A numerical–experimental methodology for simulating the aerodynamic forces acting on a moving vehicle passing through the wake of a bridge tower under cross wind. *J. Wind Eng. Ind. Aerodyn.* 104–106, 256–265.

Trias, F. and O. Lehmkuhl (2011). A self-adaptive strategy for the time integration of Navier–Stokes equations. *NUMER HEAT TR B-FUND* 60, 116–134.

Tsubokura, M., T. Nakashima, M. Kitayama,Y. Ikawa, D. H. Doh and T. Kobayashi (2010). Large eddy simulation on the unsteady aerodynamic response of a road vehicle in transient. *Int. J. Heat Fluid Fl* 31, 1075-1086.

Tsuei, L., O. Savas (2001). Transient aerodynamics of vehicle platoons during in-line oscillations. *J. Wind Eng. Ind. Aerodyn.* 13, 1085-1111.

Valerie, F. (2014). Forces and Flow Structures on a Simplified Car Model Exposed to an Unsteady Harmonic Crosswind. *ASME: J. Fluids Eng.* 136, 1-8.

Verstappen, R. and A. Veldman (2002). Symmetry-preserving discretization of turbulent flow. *J. Comp Phys.* 21, 107-114.

Volpe, R, V. Ferrand, A. D. Silva and L. Le Moyne (2014). Forces and flow structures evolution on a car body in a sudden crosswind. *J. Wind Eng. Ind. Aerodyn.* 128,114-125.

Wang, Y., Y. Xin, Z. Gu, S. Wang, Y. Deng and X. Yang (2014). Numerical and Experimental Investigations on the Aerodynamic Characteristic of Three Typical Passenger Vehicles. *J. APPL FLUID MECH* 7(4), 659-671.

Zhu, L. D., L. Li, X. U. YL and *et al*. (2010). Wind tunnel investigations of aerodynamic coefficients of road vehicles on bridge deck. *J. Fluid Struct* 22(2), 283.